Acta Crystallographica Section B
Structural Science
ISSN 0108-7681

Structural basis for the phase transitions of Cs_2HgCl_4

Bagautdin Bagautdinov,[a]† Andreas Jobst,[b] Jens Ludecke[b] and Sander van Smaalen[b]*

[a]Himeji Institute of Technology, Department of Life Science, 3-2-1 Koto, Kamigori-cho, Ako-gun, Hyogo 678-1297, Japan, and [b]Laboratory of Crystallography, University of Bayreuth, D-95440 Bayreuth, Germany

† Permanent address: Institute of Solid State Physics, Russian Academy of Sciences, Chernogolovka, Moscow District 142432, Russia.

Correspondence e-mail: smash@uni-bayreuth.de

Received 15 August 2000
Accepted 15 December 2000

The $a_0 \times b_0 \times 2c_0$ twofold superstructure of dicaesium mercury tetrachloride, Cs_2HgCl_4, at T = 120 K has been determined by single-crystal X-ray diffraction using synchrotron radiation. Lattice parameters were found as a = 9.7105 (2), b = 7.4691 (1), c = 26.8992 (4) Å, and β = 90.368 (1)° with the supercell space group $P2_1/c$. Refinements on 1828 observed unique reflections converged to R = 0.053 (wR = 0.057) using anisotropic temperature factors for all atoms. This phase is the stable phase of Cs_2HgCl_4 below 163 K. A quantitative comparison is made of the distortions of the $2c_0$ superstructure with the undistorted phase that is stable at room temperature, and with the $3c_0$ and $5a_0$ superstructures that are stable at temperatures between 163 K and room temperature. The principal difference between the $2c_0$ superstructure and all other phases of Cs_2HgCl_4 is that the Cs cations are displaced away from the centers of their coordination polyhedra in the $2c_0$ superstructure. The structural basis for the driving force of the series of phase transitions in this compound is found in the variations of the environments of Cs atoms and in the variations of the distortions of the $HgCl_4$ tetrahedra.

1. Introduction

Cs_2HgCl_4, dicaesium mercury tetrachloride, belongs to the family of A_2BX_4 compounds, which are isostructural to β-K_2SO_4. Their crystal structures are pseudohexagonal with the space group *Pnma* at high temperatures. It has been established by various experimental techniques that Cs_2HgCl_4 exhibits a sequence of seven phase transitions on cooling down from room temperature to 163 K (Dmitriev *et al.*, 1988; Kallaev *et al.*, 1990). Different commensurate and incommensurate superstructures have been identified, which correspond to modulations along either the **a** axis or the **c** axis of the underlying basic structure with *Pnma* symmetry (Table 1; Bagautdinov & Brown, 2000). At T = 221 K an incommensurate modulation parallel to **a*** appears, which locks into a $5a_0$ superstructure at 195 K. At 184 K the modulation wavevector switches from parallel **a*** to parallel **c***, and on further cooling $3c_0$, $5c_0$, incommensurate, and $7c_0$ superstructures appear, until finally the $2c_0$ superstructure develops below T_c = 163 K. It remains the stable superstructure down to at least 4.2 K (Bagautdinov & Brown, 2000).

The most typical series of phase transitions of A_2BX_4 compounds comprise the transformation from the pseudohexagonal structure at room temperature towards an incommensurately modulated phase with $\mathbf{q} = \alpha\mathbf{a}^*$, followed by a

Table 1
The various phases of Cs_2HgCl_4 as a function of temperature.

The regions of stability of the various phases are indicated together with their modulation wavevectors and symmetry.

Temperature range (K)	Wavevector	Space group
$T > 295$–221	Normal	*Pnma*
221–195	Incommensurate, $\mathbf{q} = (1/5 + \delta)\mathbf{a}^*$	$Pnma(\alpha 00)0ss$
195–184	Commensurate, $\mathbf{q} = 1/5\mathbf{a}^*$	$Pn2_1a$
184–175	Commensurate, $\mathbf{q} = 1/3\mathbf{c}^*$	$P112_1/a$
175–172	Commensurate, $\mathbf{q} = 2/5\mathbf{c}^*$	$P2_1/n11$
172–169	Incommensurate, $\mathbf{q} = (3/7 - \delta)\mathbf{c}^*$	$Pnma(0,0,\gamma)0s0$
169–163	Commensurate, $\mathbf{q} = 3/7\mathbf{c}^*$	$P2_12_12_1$
$T < 163$	Commensurate, $\mathbf{q} = 1/2\mathbf{c}^*$	$P12_1/c1$

lock-in transition resulting in a rational value of α (Cummins, 1990). The structural distortions of both the commensurate and incommensurate superstructures have been related to the Σ_2 normal mode of the space group *Pnma* (Iizumi *et al.*, 1977). Then, the structural distortions can be described as displacements of the Cs atoms in the directions perpendicular to the mirror planes together with rotations of the $HgCl_4$ tetrahedra about axes contained in the mirror planes. The very short A—X distances were proposed to be the driving force for the formation of superstructures (Fabry & Perez-Mato, 1994), and the shifts and rotations would be responsible for a relaxation of this internal strain.

A special feature of Cs_2HgCl_4 is that the direction of the modulation switches from **a*** to **c***. Obviously, the structures of the **c**-modulated phases cannot be described by the Σ_2 normal mode. Therefore, it is interesting to compare the distortions of Cs_2HgCl_4 with the distortions of the other A_2BX_4 compounds, in order to search for a common underlying principle that might be responsible for the observed phase transitions. We have performed this for the normal *Pnma*, the $5a_0$ superstructure and the $3c_0$ superstructure of Cs_2HgCl_4 in previous publications (Bagautdinov *et al.*, 1998, 1999). It was shown that the $5a_0$ superstructure involves distortions of the $HgCl_4$ tetrahedra in addition to the above-mentioned rotations and the shifts of the Cs atoms. These distortions are resolved in the $3c_0$ superstructure, but at the expense of shifts of complete tetrahedra out of the mirror planes. These findings proved that both superstructures were essentially different from the types of distortions that were thought to be responsible for the formation of superstructures in A_2BX_4 compounds (Fabry & Perez-Mato, 1994).

The $2c_0$ superstructure of Cs_2HgCl_4 is the stable structure at very low temperatures. Within the series of superstructures it is of particular interest, because it is the structure with the lowest lattice energy. The analysis of this structure will show the environments of Cs and Hg which are most favorable within the A_2BX_4 structure type and it might guide towards the finding of the true driving force for the formation of superstructures in these compounds. For these reasons, we present here the $2c_0$ superstructure of Cs_2HgCl_4 as determined by X-ray scattering at 120 K. It will be shown that the driving force for the phase transitions is to resolve the underbonding

Table 2
Experimental details.

Crystal data	
Chemical formula	Cs_2HgCl_4
Chemical formula weight	608.2
Cell setting, space group	Monoclinic, $P2_1/c$
a, b, c (Å)	9.7105 (2), 7.4691 (1), 26.8992 (4)
β (°)	90.368 (1)
V (Å^3)	1950.92 (6)
Z	8
D_x (Mg m^{-3})	4.14
Radiation type	Synchrotron
Wavelength (Å)	0.71073
μ (mm^{-1})	29.853
Crystal form, colour	Bar, colourless
Crystal size (mm)	0.15 × 0.08 × 0.04
Data collection	
Diffractometer	Huber
Data collection method	Rotation image scans
Absorption correction	Empirical
No. of measured, independent and observed parameters	6584, 2628, 1828
R_{int}	0.0627
θ_{max} (°)	30.72
Range of h, k, l	$-9 \rightarrow h \rightarrow 9$ $-10 \rightarrow k \rightarrow -1$ $-27 \rightarrow l \rightarrow 21$
Refinement	
Refinement on	F
R, wR, S	0.0529, 0.057, 1.49
No. of reflections and parameters used in refinement	2628, 129
Weighting scheme	$w = 1/[\sigma^2(F) + 0.000225F^2]$
$(\Delta/\sigma)_{max}$	0.0005
Extinction method	B–C type 1 Gaussian isotropic
Extinction coefficient	0.0016 (5)

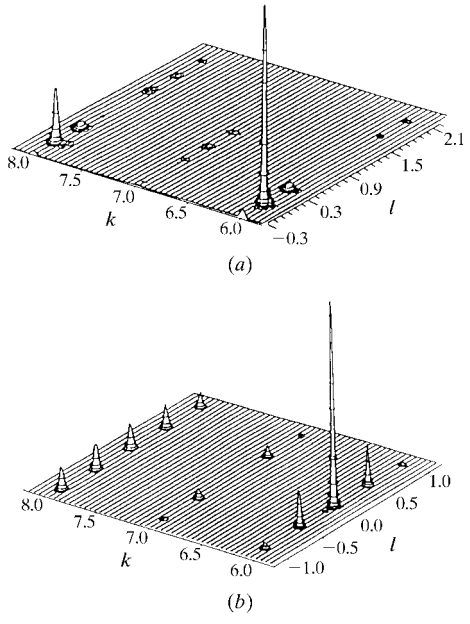

Figure 1
Two-dimensional intensity distribution in sections of the (0kl) plane at (*a*) 176 K ($3c_0$ superstructure) and (*b*) 135 K ($2c_0$ superstructure).

Table 3
Temperature dependence of the bond lengths and bond angles of the $HgCl_4$ tetrahedral groups.

Roman numerals indicate the consecutive atoms along the supercell directions in the $5a_0$, $3c_0$ and $2c_0$ supercells, respectively.

		$5a_0$ superstructure					$3c_0$ superstructure			$2c_0$superstructure	
	Pnma	I	II	III	IV	V	I	II	III	I	II
Interatomic Hg—Cl distances (Å)											
Hg—Cl(1)	2.399	2.512	2.431	2.309	2.325	2.452	2.420	2.408	2.417	2.408	2.410
Hg—Cl(2)	2.471	2.461	2.350	2.431	2.566	2.597	2.489	2.473	2.477	2.505	2.467
Hg—Cl(3)	2.456	2.456	2.479	2.503	2.445	2.435	2.476	2.465	2.463	2.511	2.505
Hg—Cl(4)	2.456	2.446	2.432	2.471	2.470	2.494	2.441	2.481	2.483	2.446	2.487
Average	2.446	2.474	2.423	2.429	2.452	2.495	2.457	2.457	2.460	2.467	2.467
Max–min	0.072	0.056	0.129	0.194	0.241	0.162	0.169	0.073	0.066	0.103	0.095
Angles (°) of the $HgCl_4$ tetrahedron											
Cl(1)—Hg—Cl(2)	118.2	119.5	118.0	117.4	119.5	120.9	118.7	119.0	118.6	117.3	116.6
Cl(1)—Hg—Cl(3)	112.7	110.0	112.1	114.6	114.7	110.7	111.0	109.8	117.0	105.3	106.8
Cl(1)—Hg—Cl(4)	112.7	114.6	115.1	112.3	109.8	111.4	113.7	114.5	109.8	124.3	117.0
Cl(2)—Hg—Cl(3)	103.3	105.0	101.7	101.1	103.3	106.3	103.1	105.6	102.4	104.7	109.5
Cl(2)—Hg—Cl(4)	103.3	101.4	104.0	105.9	104.1	101.2	104.6	102.4	104.2	102.1	103.5
Cl(3)—Hg—Cl(4)	105.5	105.0	104.3	104.2	104.1	104.9	104.3	104.3	103.0	100.4	102.9
Max–min	14.9	18.1	16.2	16.3	16.2	19.8	15.6	16.6	16.1	23.9	14.1
Bond valences between Hg and Cl											
Hg—Cl(1)	0.671	0.494	0.615	0.856	0.819	0.581	0.634	0.655	0.639	0.655	0.651
Hg—Cl(2)	0.552	0.567	0.766	0.615	0.427	0.393	0.526	0.549	0.543	0.504	0.551
Hg—Cl(3)	0.575	0.575	0.540	0.506	0.592	0.609	0.545	0.561	0.564	0.496	0.501
Hg—Cl(4)	0.575	0.561	0.614	0.552	0.554	0.519	0.599	0.537	0.535	0.591	0.529
Bond-valence sum of Hg cation (calculated directly from each Hg—Cl bond)											
Hg	2.373	2.197	2.535	2.529	2.392	2.201	2.304	2.302	2.281	2.246	2.232
Bond-valence sum of Hg cation (calculated from average Hg—Cl bond)											
Hg	2.361	2.192	2.516	2.476	2.324	2.072	2.296	2.296	2.276	2.232	2.232

of the 11-coordinated Cs atoms. The series of phase transitions is explained by the observation that the most stable environment of Cs can only be reached at the expense of an environment of the Hg atoms, which is less favourable.

2. Experimental

The present X-ray scattering experiment used the same crystal as was used in our previous experiments (Bagautdinov *et al.*, 1999). X-ray scattering was measured with synchrotron radiation at beamline F1 of Hasylab at DESY (Hamburg, Germany), using a Siemens SMART CCD camera as the detector. The specimen was cooled by a nitrogen flow cryostat and was kept at 120.0 (5) K for the present data collection. Details of the experiment are summarized in Table 2. The extraction of integrated intensities and data reduction were performed with the standard Siemens-CCD software (*SAINT*; Siemens, 1996) and with *SADABS* (Sheldrick, 1996).

The lattice was found to be monoclinic and the crystal appeared to be twinned with both orientations of the monoclinic structure present within the orthorhombic lattice. Parameters for the integration were chosen such that a sum of intensities of the two domains was obtained for each diffraction maximum. The scattering was dominated by one domain with a refined occupation fraction of 0.829 (2). Analysis of the extinction rules on the 1828 unique reflections indicated the space group $P2_1/c$ (b axis unique), which is a subgroup of *Pnma*. On average, the $2c_0$ superstructure reflections have the same intensity as the main reflections (Fig. 1). Thus, the distortions cannot be considered as small deviations from the basic structure, as was true for other superstructures.

Lattice parameters were determined on a Nonius Mach-3 CAD-4 (Mo $K\alpha$ radiation) from the setting angles of 25 reflections in the range $18 < \theta < 24°$. Monoclinic lattice parameters were found to be a = 9.7105 (2), b = 7.4691 (1), c = 26.8992 (4) Å, and β = 90.368 (1)° with the supercell space group $P2_1/c$. The volume of the unit cell of the $2c_0$ superstructure at 120 K is slightly less than twice the volume of the unit cell a_0, b_0, c_0 at room temperature, but an anomalous change of the lattice parameters is observed: both a and b are smaller at 120 K than at room temperature, while $c_0 = c/2$ at 120 K is larger than c_0 at room temperature by 0.06 Å.

The refinement of the twofold superstructure began with atoms at the positions equal to those of the structure at room temperature (Bagautdinov *et al.*, 1998), but was recalculated for the double unit cell. With small shifts applied to these coordinates, the refinement proceeded smoothly to a good fit with R = 0.057 (Table 2). Refinements were carried out with the program *JANA*2000 (Petricek & Dusek, 2000). Each reflection (h,k,l) was assumed to be the weighted sum of intensities of the (h,k,l) and ($\bar{h}$,k,l) reflections, using the twinning option in *JANA*2000 (Petricek & Dusek, 2000). Details on the refinement are summarized in Table 2. Final atomic coordinates and displacement parameters have been deposited.[1]

[1] Supplementary data for this paper are available from the IUCr electronic archives (Reference: CK0002). Services for accessing these data are described at the back of the journal.

Table 4
Fractional displacements and the magnitudes of the shift vector (Å) of atoms in the $2c_0$ superstructure at 120 K compared with their positions in the normal phase at room temperature.

Atoms	*x* axis	*y* axis	*z* axis	Length of the shift
Cs(1)	−0.0050	0.0048	−0.0074	0.2077
Cs(2)	0.0052	0.0065	−0.0040	0.1287
Hg(1)	−0.0095	0.0183	−0.0025	0.1779
Cl(1)	−0.0065	0.0928	−0.0090	0.7368
Cl(2)	0.0053	0.0016	−0.0007	0.0562
Cl(3)	0.0029	0.0290	0.0021	0.2256
Cl(4)	−0.0147	−0.0051	0.0014	0.1527
Cs(1*a*)	0.0004	−0.0211	0.0130	0.3836
Cs(2*a*)	0.0015	0.0343	0.0020	0.2622
Hg(1*a*)	−0.0013	−0.0302	0.0013	0.2286
Cl(1*a*)	0.0024	−0.0174	0.0007	0.1333
Cl(2*a*)	−0.0020	0.0523	0.0046	0.4103
Cl(3*a*)	0.0132	−0.0689	0.0269	0.8965
Cl(4*a*)	−0.0090	0.0785	−0.0188	0.7788

3. Discussion

The typical superstructures of A_2BX_4 compounds comprise an increase of the *a* axis with displacements of the atoms according to the Σ_2 normal mode of the space group *Pnma* (Iizumi *et al.*, 1977). This involves displacements of the *A* atoms in the directions perpendicular to the mirror planes and rotations of the BX_4 tetrahedra about the axes contained in the mirror planes. In a previous publication we showed that the $5a_0$ superstructure of Cs_2HgCl_4 involved large deformations of the $HgCl_4$ tetrahedra and the normal mode picture of the distortion was found not to be valid in that case (Bagautdinov *et al.*, 1999).

In the $3c_0$ superstructure these distortions were resolved, but the $HgCl_4$ groups showed displacements out of the mirror planes. This was interpreted as less distorted tetrahedra being more stable and the $3c_0$ superstructure thus having lower lattice energy than the $5a_0$ superstructure, the $3c_0$ phase being the stable phase at a lower temperature.

As to be expected, thermal displacement parameters of the atoms are smaller in the $2c_0$ superstructure (see supplementary material) than they are in the structures at higher temperatures (Bagautdinov *et al.*, 1998, 1999). Remarkable is that in the $2c_0$ superstructure the anisotropy of the thermal displacement tensors is considerably reduced. This might be taken as an indication for ordering of the atoms in the low-temperature phase.

The $2c_0$ superstructure exhibits one of two independent $HgCl_4$ tetrahedra which is less distorted than any $HgCl_4$ group in any other phase, but, maybe surprisingly, the other $HgCl_4$ group has a wider range of values of the Cl—Hg—Cl bond angles than any $HgCl_4$ group in the $3c_0$ superstructure (Table 3). In addition, rotations about an axis close to the *a* axis, and shifts of the $HgCl_4$ groups perpendicular to the mirror planes, are found in this phase also (Figs. 2 and 3; Table 4). Considering the lengths of the Hg—Cl bonds, both $HgCl_4$ groups again appear more distorted in the $2c_0$ superstructure than in the $3c_0$ phase or the parent structure at room temperature (Table 3). Although we stick to our opinion that the more regular tetrahedrons represent more stable structures of individual $[HgCl_4]^{2-}$ complex anions, the observed structural features do suggest that the interactions between Hg and Cl are not the driving force for the phase transitions. It is noted that the valence of Hg as calculated with the bond-valence method is slightly lower in the $2c_0$ superstructure than at higher temperatures. We attribute this to the apparent contraction of chemical bonds as found in X-ray crystallography due to the thermal motion of the atoms at the higher temperature.

In all phases there are two types of environments for caesium. At room temperature Cs(1) has coordination 11 by Cl, and Cs(2) is in nine coordination by Cl. In the $2c_0$ superstructure the most dramatic changes are found for 11-coordinated caesium. For both Cs(1) and Cs(1*a*) the longest bonding distance Cs—Cl is increased by ∼0.5 Å compared with the similar distance in the other phases (Tables 5 and 6).

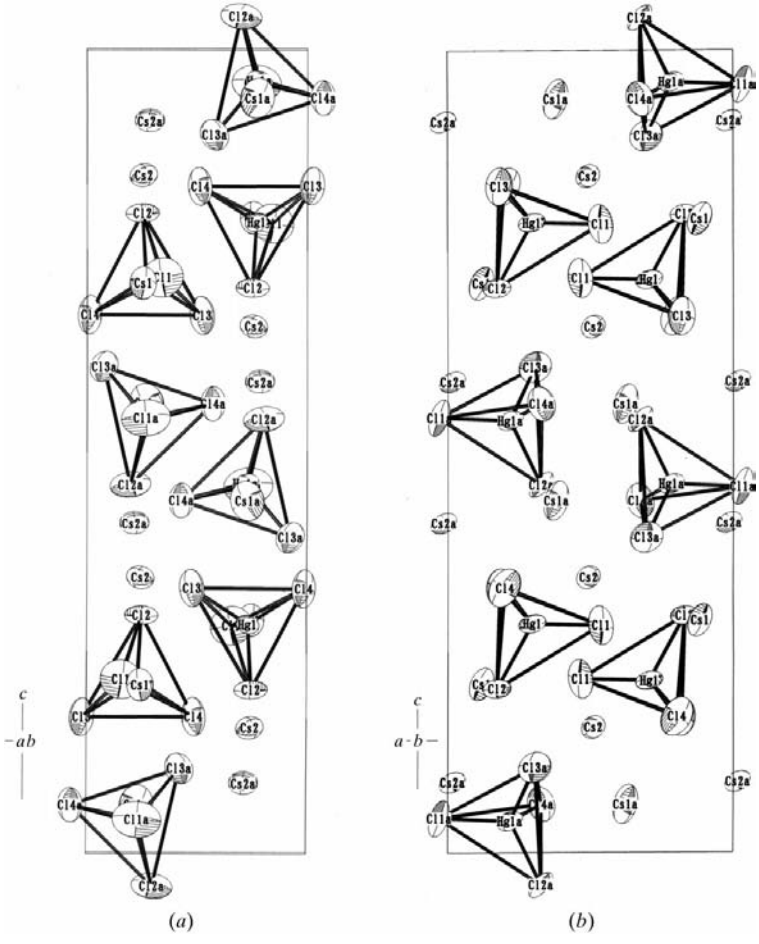

Figure 2
Projection of the $2c_0$ superstructure of Cs_2HgCl_4 onto (*a*) the (100) and (*b*) the (010) planes. The atoms are represented by ellipsoids with 50% probability level. Cl—Cl connections are shown to illustrate the $HgCl_4$ tetrahedra.

Table 5
Interatomic distances (Å) and bond valences between the Cs and Cl atoms.

The bond-valence values (v) were calculated using the parameters from Brown & Altermatt (1985).

	Distances	v
Cs(1)—Cl(1)^{i}	3.439 (8)	0.174
Cs(1)—Cl(2)	3.614 (8)	0.108
Cs(1)—Cl(2)^{ii}	3.798 (6)	0.066
Cs(1)—Cl(2)^{iii}	3.751 (6)	0.075
Cs(1)—Cl(3)	3.690 (7)	0.088
Cs(1)—Cl(3) ^{ii}	3.744 (8)	0.076
Cs(1)—Cl(4) ^{iv}	3.849 (8)	0.057
Cs(1)—Cl(4) ^{v}	3.728 (7)	0.080
Cs(1)—Cl(1a)^{iv}	4.732 (9)	0.005
Cs(1)—Cl(3a)^{iv}	3.585 (8)	0.117
Cs(1)—Cl(4a)^{vi}	5.084 (8)	0.002
Cs(1a)—Cl(1)^{vii}	4.498 (9)	0.010
Cs(1a)—Cl(3)^{vii}	3.976 (8)	0.041
Cs(1a)—Cl(4)^{viii}	3.938 (8)	0.045
Cs(1a)—Cl(1a)^{ix}	3.394 (8)	0.196
Cs(1a)—Cl(2a)	4.002 (8)	0.038
Cs(1a)—Cl(2a)^{vii}	4.035 (6)	0.035
Cs(1a)—Cl(2a)^{x}	3.578 (6)	0.119
Cs(1a)—Cl(3a)	3.626 (7)	0.105
Cs(1a)—Cl(3a)^{x}	5.215 (8)	0.001
Cs(1a)—Cl(4a)^{xi}	3.483 (8)	0.154
Cs(1a)—Cl(4a)^{xii}	3.645 (7)	0.100
Cs(2)—Cl(1)	3.498 (9)	0.148
Cs(2)—Cl(1)^{xiii}	3.516 (7)	0.141
Cs(2)—Cl(1)^{xiv}	4.690 (7)	0.006
Cs(2)—Cl(2)	3.519 (8)	0.140
Cs(2)—Cl(3)^{xiii}	3.508 (7)	0.144
Cs(2)—Cl(4)^{vii}	3.449 (7)	0.169
Cs(2)—Cl(2a)^{xiii}	3.511 (8)	0.143
Cs(2)—Cl(3a)^{xii}	3.394 (7)	0.196
Cs(2)—Cl(4a)^{xv}	3.430 (8)	0.178
Cs(2a)—Cl(2)^{iii}	3.496 (8)	0.149
Cs(2a)—Cl(3)	3.483 (7)	0.154
Cs(2a)—Cl(4)^{xii}	3.456 (7)	0.166
Cs(2a)—Cl(1a)	3.548 (9)	0.129
Cs(2a)—Cl(1a)^{iv}	4.069 (7)	0.032
Cs(2a)—Cl(1a)^{xvi}	3.831 (7)	0.060
Cs(2a)—Cl(2a)	3.558 (7)	0.126
Cs(2a)—Cl(3a)^{xvi}	3.584 (7)	0.117
Cs(2a)—Cl(4a)^{xvii}	3.483 (7)	0.154

Symmetry codes: (i) $1+x, y, z$; (ii) $1-x, -\frac{1}{2}+y, \frac{1}{2}-z$; (iii) $1-x, \frac{1}{2}+y, \frac{1}{2}-z$; (iv) $1-x, 1-y, 1-z$; (v) $x, \frac{1}{2}-y, -\frac{1}{2}+z$; (vi) $1-x, -\frac{1}{2}+y, \frac{3}{2}-z$; (vii) $-x, 1-y, 1-z$; (vii) $-x, 1-y, 1-z$; (viii) $-x, \frac{1}{2}+y, \frac{3}{2}-z$; (ix) $-1+x, y, z$; (x) $-x, 2-y, 1-z$; (xi) $-x, -\frac{1}{2}+y, \frac{3}{2}-z$; (xii) $x, \frac{3}{2}-y, -\frac{1}{2}+z$; (xiii) $-x, -\frac{1}{2}+y, \frac{1}{2}-z$; (xiv) $-x, \frac{1}{2}+y, \frac{1}{2}-z$; (xv) $x, -1+y, -1+z$; (xvi) $1-x, 2-y, 1-z$; (xvii) $1-x, -\frac{1}{2}+y, \frac{3}{2}-z$.

This leads to the conclusion that in the $2c_0$ superstructure the coordinations of these Cs atoms are reduced towards 10. A second large effect is the definite increase of the valence of the underbonded Cs(1) atoms, when going from the room-temperature phase to the $5a_0$ and $3c_0$ superstructures, and finally towards the $2c_0$ superstructure. On the other hand, the average of the valences of Cs(2) and Cs(2a) is about equal to the corresponding values in structures at higher temperatures. Both observations support the proposition that the Cs(1)—Cl interactions represent the driving force for the phase transitions.

Fabry & Perez-Mato (1994) have shown that the phase transitions in A_2BX_4 compounds correlate with the relative contribution of the shortest $A(1)-X(1)$ bond to the bond-valence sum of the $A(1)$ cation. When this ratio is larger than 0.24 (as is the case for Cs_2HgCl_4 at room temperature) the compound is likely to undergo a phase transition towards a superstructure. Presently we find that the bond valences of this shortest Cs(1)—Cl(1) bond remain around the same value for both Cs(1) and Cs(1a) compared with the values in the other phases. Therefore, the driving force for the phase transitions cannot be to resolve too short a Cs—Cl bond. On the other hand, the calculated valences of Cs(1) and Cs(1a) have increased by 0.1 compared with the $3c_0$ phase and even by 0.17 compared with room temperature. Therefore, we conclude that a strive towards increased bonding of the underbonded Cs(1) atoms is the true driving force for the formation of the superstructures. Owing to this increased valence, the ratio of the Cs(1)—Cl(1) bond valence to the bond-valence sum of the Cs(1) happens to fall below 0.24 in the $2c_0$ superstructure (Table 6).

The other structural features then are a consequence of the deformations that are necessary to achieve the increased bonding of Cs(1). The valences of Cs atoms calculated by the bond-valence method vary much more from one phase to the other than valence values obtained from average Cs—Cl bond lengths (Table 6). This indicates that the coordination polyhedra of Cs(1) become more irregular on decreasing temperatures.

4. Conclusions

We have determined the $2c_0$ superstructure of Cs_2HgCl_4, as it was found to be the stable structure below a temperature of 163 K. Analysis of this structure and comparison with the structures of Cs_2HgCl_4 which are stable at higher temperatures have revealed that a strive towards increased bonding of the underbonded Cs(1) type of atoms is the driving force for the formation of superstructures at lower temperatures.

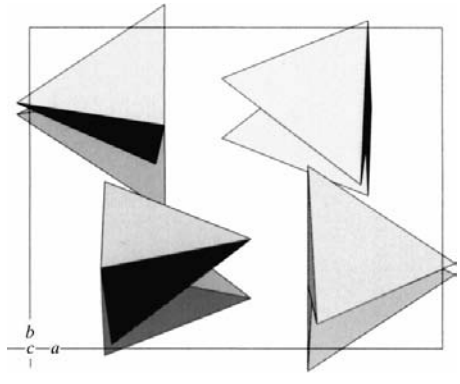

Figure 3
Projection of the $2c_0$ superstructure of Cs_2HgCl_4 onto the (001) plane. $HgCl_4$ groups are represented by shaded tetrahedra with the vertices representing the positions of the Cl atoms. Cs atoms have been omitted.

Table 6
Temperature dependence of the Cs—Cl bonds.

Roman numerals indicate the consecutive atoms along the supercell directions in the $5a_0$, $3c_0$ and $2c_0$ supercells, respectively.

	Pnma	$5a_0$ superstructure					$3c_0$ superstructure			$2c_0$ superstructure	
		I	II	III	IV	V	I	II	III	I	II
Average Cs—Cl distances (Å) at different phases											
Cs(1)—Cl	3.934	3.902	3.899	3.917	3.922	3.916	3.928	3.921	3.915	3.910	3.944
Cs(2)—Cl	3.614	3.620	3.585	3.579	3.594	3.617	3.608	3.605	3.603	3.613	3.612
The largest distances (Å) in Cs—Cl polyhedra at different phases											
Cs—Cl	4.553	4.464	4.600	4.558	4.663	4.645	4.653	4.492	4.600	5.084	5.215
Bond-valence sums of Cs cations (calculated directly from each Cs—Cl bond)											
Cs(1)	0.681	0.739	0.766	0.749	0.744	0.877	0.721	0.741	0.754	0.848	0.844
Cs(2)	1.116	1.109	1.109	1.242	1.159	1.100	1.151	1.128	1.164	1.265	1.087
Bond-valence sums of Cs cations (calculated from average Cs—Cl bond)											
Cs(1)	0.506	0.550	0.550	0.528	0.517	0.528	0.506	0.517	0.528	0.539	0.484
Cs(2)	0.972	0.954	1.053	1.071	1.083	0.963	0.999	0.999	0.999	0.981	0.981
The Cs(1)—Cl(1) bond at difference phases											
Distance (Å)	3.423	3.396	3.525	3.507	3.363	3.291	3.411	3.427	3.418	3.439	3.394
Bond valence	0.181	0.195	0.138	0.144	0.213	0.259	0.187	0.179	0.184	0.174	0.196
$v/\Sigma v$ 100%	26	26.4	18.0	19.2	28.6	29.5	25.9	24.2	24.4	20.5	23.2

We are grateful to Professor V. I. Pakhomov and Dr Yu. Yuzyuk for providing us with the single crystal of Cs_2HgCl_4. Dr W. Morgenroth is thanked for his assistance with the synchrotron experiment. Financial support was obtained from the Deutsche Forschungsgemeinschaft (DFG) and the Fonds der chemischen Industrie.

References

Bagautdinov, B. & Brown, I. D. (2000). *J. Phys. Condens. Matter*, **12**, 8111–8125.
Bagautdinov, B., Ludecke, J., Schneider, M. & van Smaalen, S. (1998). *Acta Cryst.* B**54**, 626–634.
Bagautdinov, B., Pilz, K., Ludecke, J. & van Smaalen, S. (1999). *Acta Cryst.* B**55**, 886–985.
Brown, I. D. & Altermatt, D. (1985). *Acta Cryst.* B**41**, 244–247.
Cummins, H. Z. (1990). *Phys. Rep.* **185**, 211–409.
Dmitriev, V. P., Yuzyuk, Yu. I., Tregubchenko, A. V., Larin, E. S., Kirilenko, V. V. & Pakhomov, V. I. (1988). *Sov. Phys. Solid State*, **30**, 704–705.
Fabry, J. & Perez-Mato, J. M. (1994). *Phase Transit.* **49**, 193–229.
Iizumi, M., Axe, J. D., Shirane, G. & Shimaoka, K. (1977). *Phys. Rev. B*, **15**, 4392–4411.
Kallaev, S. N., Gladkii, V. V., Kirikov, V. A. & Kamilov, I. K. (1990). *Ferroelectrics*, **106**, 299–302.
Petricek, V. & Dusek, M. (2000). *JANA*2000. Institute of Physics, Academy of the Czech Republic, Praha, Czech Republic.
Sheldrick, G. M. (1996). *SADABS*. University of Göttingen, Germany.
Siemens (1996) *SAINT*. Siemens Analytical X-ray Instruments Inc., Madison, Wisconsin, USA.